

Electronic and Magnetic Properties of Ultrathin Au/Pt Nanowires

Xiaowei Teng,^{*,†} Mikhail Feygenson,[‡] Qi Wang,[§] Jiaqing He,^{||} Wenxin Du,[†] Anatoly I. Frenkel,[§] Weiqiang Han,[⊥] and Meigan Aronson^{‡,#}

Department of Chemical Engineering, University of New Hampshire, Durham, New Hampshire 03824, Condensed Matter Physics and Materials Science Department, Center for Functional Nanomaterials, Brookhaven National Laboratory, Upton, New York 11973, Department of Physics, Yeshiva University, New York, New York 10016, Department of Materials Science and Engineering, Northwestern University, Evanston, Illinois 60208, and Department of Physics and Astronomy, State University of New York, Stony Brook, New York 11794

Received April 29, 2009; Revised Manuscript Received July 14, 2009

ABSTRACT

We have reported the synthesis of $\text{Au}_{25}\text{Pt}_{75}$ and $\text{Au}_{48}\text{Pt}_{52}$ alloyed ultrathin nanowires with average widths of less than 3 nm via a wet chemistry approach at room temperature. Using a combination of techniques, including scanning transmission electron microscopy equipped with X-ray energy dispersive spectroscopy, ultraviolet–visible spectroscopy, and X-ray absorption near-edge structure and extended X-ray absorption fine structure spectroscopies, we identified the stoichiometry-dependent heterogeneous crystalline structures, as well as electronic structures with respect to the charge transfer between Pt and Au within both nanowires. In particular, we observed d-charge depletion at the Au site and the d-charge gain at the Pt site in $\text{Au}_{48}\text{Pt}_{52}$ nanowires, which accounted for its ferromagnetic magnetic behavior, in contrast to the paramagnetism and diamagnetism appearing respectively in bulk Pt and Au.

Magnetic materials have been used in various technologically important areas for many years, including magnetic fluids, catalysis, biotechnology/biomedicine, magnetic resonance imaging, data storage, and environmental remediation.^{1–8} By carefully tuning the size of the materials down to the nanoscale, new magnetic properties emerge that do not appear in their bulk counterparts. In general, the energy of a magnetic material depends on the local environment of the magnetic atoms via the crystal electric field, known as magnetic anisotropy, analogous to the magnetocrystalline anisotropy characteristic of bulk, equilibrium magnetic materials. In bulk three-dimensional (3D) material, the orbital momentum of the electrons, quenched by the crystal electric field, is very small compared with the spin moment. Consequently, the spin–orbital coupling appears only as perturbation in determining the magnetic moment of a bulk material. However, when the size of the magnetic system is reduced to the nanoscale, more atoms will be located at or

very near the surface. Accordingly, the quenching of the orbital moments may be suppressed, leading to the resurrection of the moment at lower coordinated surfaces. This induces, via spin–orbital coupling, an extra contribution to the magnetic anisotropy energy, the so-called surface anisotropy first named by Néel.^{9,10} Enhancing the magnetic anisotropy energy in small particles by introducing surface anisotropy brings a stronger tendency toward ferromagnetism to transition metals that are normally nonmagnetic, displaying only Pauli paramagnetism or diamagnetic behavior.

Magnetic properties of two-dimensional (2D) thin films and zero-dimensional (0D) nanoparticles have been intensively studied. Because of the dramatic size and dimensionality effects in nanoscale, the unusual ferromagnetism found among them has become one of the most attractive issues recently.^{11–25} In a confined system, reduced coordination favors narrower electron bands and yields a larger density of states at the Fermi level $N(E_F)$ relative to the bulk, leading in some cases to the satisfaction of Stoner criterion for ferromagnetism, $N(E_F) \cdot J > 1$ (J is exchange integral).²⁶ For example, palladium (Pd) bulk metal is paramagnetic, because its d band is too wide and its density of states is too small to satisfy the Stoner criterion. However, ferromagnetic behavior has been observed in twinned Pd nanoparticles with a diameter of 2.4 nm.¹⁸ This unusual ferromagnetism has

* To whom correspondence should be addressed. Tel: 603-8624245. Fax: 603-8622486. E-mail: xw.teng@unh.edu.

[†] University of New Hampshire.

[‡] Condensed Matter Physics and Materials Science Department, Brookhaven National Laboratory.

[§] Yeshiva University.

^{||} Northwestern University.

[⊥] Center for Functional Nanomaterials, Brookhaven National Laboratory.

[#] State University of New York.

been attributed to the emerging surface anisotropy of Pd atoms, especially those located in the vicinity of the twin boundary. Size-dependent ferromagnetic properties have also been observed in gold (Au), which is diamagnetic in bulk. Hori et al. reported that Au nanoparticles with an average diameter of 3 nm exhibited the highest magnetization, while particles with diameters larger than 4 nm displayed magnetic behavior consistent with that of the bulk metal.²¹ Because the characteristic length scales of physical factors giving rise to surface anisotropy are only a few nanometers, the key to observe novel nanomagnetism in materials that are normally nonmagnetic in the bulk is to achieve a large scale synthesis of free-standing nanomaterials with a high level of uniformity and small sizes.

Besides morphological effects, unconventional magnetic properties in nanomaterials are also dependent to a great extent on the electronic structure. Litran et al. showed experimentally that charge transfer between Pd nanoparticles and surrounding capping agents could induce ferromagnetic behavior in Pd. When tetraalkylammonium salt or alkyl thiol was used as capping agents, a high degree of surface oxidation of the Pd nanoparticles resulted, due to the strong interaction between Pd and the stabilizing agents. Consequently, the 4d density of holes at the Pd site was increased, leading to the formation of a localized magnetic moment which enabled ferromagnetism for a large temperature range.²³ Similar observations have been recently found in Au, Ag, Cu, and ZnO nanoparticles.^{24,25,27–34} When those nanomaterials were capped by surfactants such as alkyl thiols and amines, charge transfer from the metal atoms to S and N with the generation of holes in d orbitals, giving rise to ferromagnetic moments at temperatures as large as 300 K.

Bimetallic nanostructures are of increasing scientific importance, because it is possible to enhance or to obtain new magnetic behaviors that cannot be obtained in single component nanostructure. It is well known that the physical properties of bimetallic nanomaterials depend strongly on their crystalline structures, for instance whether or not the two monometallic elements are chemically segregated or intimately alloyed. However, fundamental understanding of structure-magnetic property correlations in nanomagnetic materials is still lacking. Particularly, the nature of the magnetic response and the dependence of ferromagnetic behavior on the crystalline nanostructure are fundamental and unresolved issues. Among various bimetallic nanomaterials, Au/Pt has attracted special interest. Although both pure Au and Pt can be ferromagnetic in nanosized particles, the magnetic properties of their alloyed form have not previously been reported. In this context, one challenge in the synthesis and characterization of Au/Pt materials is their stoichiometry-dependent crystalline structure. Even though the mismatch of the lattice constants between Pt and Au is small (3.92 Å vs 4.08 Å), the bulk solubility of Au in Pt is only 4% at room temperature, and no more than 6% at 973 K.³⁵ Because of a miscibility gap in the Au/Pt, it is not possible to form homogeneous bulk alloys with the compositions achieved in nanosystems, where Pt and Au atoms can reach diffusion equilibrium more easily than in the bulk,

promoted by the fast and spontaneous reduction of Pt and Au precursors in solution.^{36–38} Nevertheless, the synthesis of AuPt alloy nanomaterials is still not trivial. Careful control over stabilizing agents, the reducing agent and the reaction procedure is essential. The synthesis of uniform 1D AuPt ultrathin nanowires and the investigation of their magnetic behaviors have, to our knowledge, not been reported to date.

In this paper we report the synthesis of Au/Pt alloy nanowires with different stoichiometries via a wet chemistry approach. By taking advantage of combined characterization techniques, including scanning transmission electron microscopy (STEM) equipped with X-ray energy dispersive spectroscopy (EDS), ultraviolet–visible (UV–vis) spectroscopy, and synchrotron-based X-ray absorption near-edge structure (XANES) and extended X-ray absorption fine structure (EXAFS) spectroscopies, we identified the nature of heterogeneous nanostructures of as-made Au₄₈Pt₅₂ and Au₂₅Pt₇₅ alloyed nanowires. We also concluded that homogeneous alloying between Pt and Au in Au₄₈Pt₅₂ nanowires modified the electronic structures of both metals and caused d-charge depletion at the Au site, accompanied by d-charge gain at the Pt site, resulting in an induced ferromagnetic moment of Au. This result sheds light on the correlation between charge transfer and the origin of ferromagnetism in nanoscaled metals that are normally nonmagnetic.

Au/Pt nanowires were prepared by a phase transfer method, in which inorganic precursors gold chloride (AuCl₃) and sodium tetrachloroplatinate (Na₂PtCl₄) were transferred into an organic mixture of octadecylamine and toluene via a phase transfer agent (*n*-dodecyltrimethylammonium bromide).³² Subsequent injection of the reducing agent sodium tetrahydroborate (NaBH₄) aqueous solution resulted in the formation of ultrathin Au/Pt nanowires. Electron microscopy images were acquired using Zeiss/LEO 922 Omega TEM and JEOL 2100 STEM equipped with EDS, respectively. The chemical compositions of Au/Pt nanowires were analyzed by EDS measurements for a nanowire assembly that covered an area of ~1 μm². The EDS spectra showed average elemental compositions of Au₄₈Pt₅₂ and Au₂₅Pt₇₅ (see Supporting Information Figure S1). Conventional bright field images of Au₄₈Pt₅₂ and Au₂₅Pt₇₅ are shown in Figure 1. Au₄₈Pt₅₂ and Au₂₅Pt₇₅ nanowires exhibited a uniform 1D morphology with average lengths as large as 100 nm, average widths of 2.6 ± 0.4 nm and 2.5 ± 0.3 nm, respectively. The Au/Pt nanowires appeared to be entirely crystalline, evidenced by the lattice fringes that extend across the full extent of the TEM image. Dominant lattice spacings of 2.30 Å were obtained, which corresponds to the interplanar distances of the (111) Au/Pt surfaces. In general, the shape of materials is highly dependent on competitive growth along the low index crystal planes in the presence of surfactant, including [111], [110], and [100].^{39–50} Anisotropic growth of Au/Pt nanowires is rather unexpected due to the symmetric cubic lattices of both Pt and Au metals. However, our TEM data indicate that octadecylamine might preferentially adsorb on the²² surfaces of Au and Pt, facilitating the growth of Au/Pt nanowires along the <111> directions.

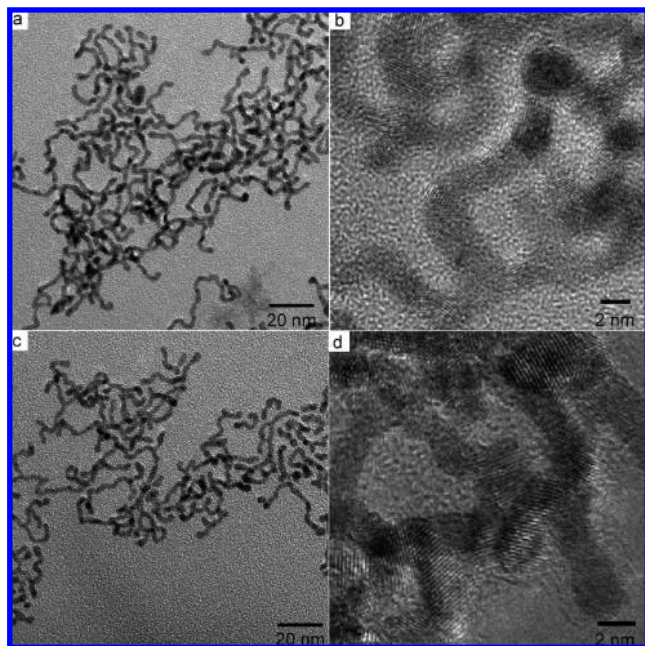


Figure 1. Bright-field TEM images of (a,b) $\text{Au}_{48}\text{Pt}_{52}$ and (c,d) $\text{Au}_{25}\text{Pt}_{75}$ nanowires.

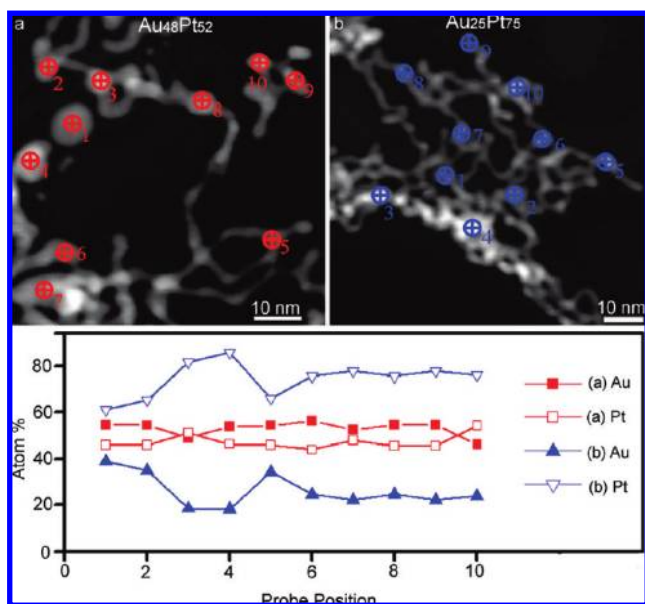


Figure 2. The dark-field images of $\text{Au}_{48}\text{Pt}_{52}$ and $\text{Au}_{25}\text{Pt}_{75}$ nanowires, and the elements distributions along individual nanowire assessed by STEM-EDS analysis.

The distributions of the elements along individual nanowires were also assessed by the probe analysis in the STEM-EDS mode as shown in Figure 2. As illustrated, the contents of Pt and Au were determined at 10 sites for either nanowire. Average chemical compositions of $\text{Au}_{53\pm3}\text{Pt}_{47\pm3}$ and $\text{Au}_{26\pm7}\text{Pt}_{74\pm7}$ were identified. The close correspondence of the EDS analysis results obtained from individual nanowires and from their large area assemblies, demonstrates the high degree of homogeneity in chemical composition over a large quantity of as-made $\text{Au}_{48}\text{Pt}_{52}$ and $\text{Au}_{25}\text{Pt}_{75}$ nanowires.

We also performed a UV-vis absorption study of pure Pt, $\text{Au}_{48}\text{Pt}_{52}$, and $\text{Au}_{25}\text{Pt}_{75}$ nanowires as shown in Figure S2

(Supporting Information). As expected, pronounced absorption peaks characteristic of gold are obtained for $\text{Au}_{48}\text{Pt}_{52}$ and $\text{Au}_{25}\text{Pt}_{75}$. Moreover, the intensity of the surface plasmon resonance (SPR) peak of gold was more pronounced and shifted to higher wavelength in the gold-rich $\text{Au}_{48}\text{Pt}_{52}$. This spectroscopic evidence further confirmed the increased alloying of Au with Pt from $\text{Au}_{25}\text{Pt}_{75}$ to $\text{Au}_{48}\text{Pt}_{52}$.^{45,51} Although we intended to synthesize Au/Pt nanowires with higher Au atomic ratios, instead a mixture of nanowires and spherical nanoparticles with various sizes was obtained (Supporting Information Figure S3). The UV-vis absorption performed on this mixture showed a broadened peak between 510 and 550 nm, indicating the coexistence of Au/Pt and Au nanomaterials. Our observation that it is possible to form Au/Pt ultrathin nanowires which are 2–3 nm in width where the solubility of Au in Pt is as large as 48 atomic % (in $\text{Au}_{48}\text{Pt}_{52}$ nanowires is conclusive evidence that the Au/Pt binary phase diagram is qualitatively different for nanoscaled systems). $\text{Au}_{48}\text{Pt}_{52}$ appears to be near the upper limit of the solubility of Au in Pt in ultrathin nanowires, beyond which phase segregation occurs. To synthesize Au/Pt alloy materials with even higher Au ratio, ultrathin nanowires or ultrasmall nanoparticles with width or dimension less than 2 nm might be required.

Although the morphology and chemical structure of Au/Pt alloy nanowires were verified by TEM and EDS, details of the precise crystalline structure such as the Au and Pt distribution and/or coordination inside the nanowires, which is crucial to its physical properties, has not been determined. Further detailed analysis was conducted by EXAFS studies. EXAFS is a well-established tool for investigating the structure of bimetallic nanomaterials, since the local environment of atoms of each resonant element can be studied separately by tuning the X-ray energy to the absorbing edge of each metal.^{52,53} EXAFS experiments were performed at both Pt L_3 and Au L_3 edges. In addition to the Au/Pt alloyed nanowires, Au and Pt foils were measured simultaneously with the nanowire samples in reference mode for X-ray energy calibration and data alignment at each absorption edge. Theoretical analysis, using IFEFFIT package⁵⁴ and FEFF6 software,⁵⁵ was done by simultaneous fitting of both the Pt and Au edge data while accurately accounting for the Pt contribution in Au EXAFS that overlap in the same X-ray energy region.^{56,57} The Fourier transform magnitudes of k^2 -weighted EXAFS data and theoretical fits for Pt and Au L_3 edges of $\text{Au}_{25}\text{Pt}_{75}$ and $\text{Au}_{48}\text{Pt}_{52}$ are shown in Supporting Information, Figure S4. The best fit values of structural parameters (coordination numbers, first nearest neighbor distances and their mean squared disorders, σ^2) are listed in the Table 1. For $\text{Au}_{48}\text{Pt}_{52}$ nanowires, the first-nearest-neighbor (1NN) Pt-metal coordination number ($N_{\text{Pt-M}} \equiv N_{\text{Pt-Au}} + N_{\text{Pt-Pt}}$) is 9.1 ± 0.6 , comparable to that of Au-metal coordination number ($N_{\text{Au-M}} \equiv N_{\text{Au-Pt}} + N_{\text{Au-Au}} = 9.7 \pm 1.9$). The fact that $N_{\text{Pt-M}} \approx N_{\text{Au-M}}$ within the error bars implies the formation of a homogeneous Au/Pt alloy. Thus, Au or Pt do not segregate to different macroscopic regions within the nanostructure (e.g., to the center or surface). Our measurements of $\text{Au}_{25}\text{Pt}_{75}$ nanowires suggest a heterogeneous

Table 1. Best Fit Results Obtained by EXAFS Analysis for Au/Pt Bimetallic Nanowires

samples	Pt foil	Au ₂₅ Pt ₇₅	Au ₄₈ Pt ₅₂	Au foil
$N_{\text{Pt-M}}$	12 ^a	5.3 (6)	9.1 (6)	
$N_{\text{Au-M}}$		9.4 (1.9)	9.7 (1.9)	12 ^a
$N_{\text{Pt-O}}$		0.8 (7)		
$N_{\text{Au-O}}$		0.9 (5)		
$R_{\text{Pt-M}}(\text{\AA})$	2.775 (2)	2.750 (6)	2.767 (5)	
$R_{\text{Au-M}}(\text{\AA})$		2.84 (1)	2.82 (1)	2.877 (3)
$R_{\text{Pt-O}}(\text{\AA})$		1.95 (4)		
$R_{\text{Au-O}}(\text{\AA})$		1.77 (2)		
$\sigma_{\text{Pt-M}}^2(\text{\AA}^2)$	0.0050 (1)	0.0024 (4)	0.0105 (8)	
$\sigma_{\text{Au-M}}^2(\text{\AA}^2)$		0.0075 (11)	0.0086 (18)	0.0081 (2)
$\sigma_{\text{Pt-O}}^2(\text{\AA}^2)$		0.0077 (140)		
$\sigma_{\text{Au-O}}^2(\text{\AA}^2)$		0.0029 (52)		

^a INN coordination number was fixed at 12 for Pt and Au bulk standard analyses.

distribution of Au and Pt atoms inside the nanowires. The observed relationship: $N_{\text{Pt-M}}(5.3 \pm 0.6) < N_{\text{Au-M}}(9.4 \pm 1.9)$ indicates that Au atoms tend to segregate toward the core of the Au₂₅Pt₇₅ nanowires, leading to a heterogeneous nanostructure with a Au rich and highly coordinated core and a less-coordinated and Pt-rich shell, since the atoms on the surface have fewer neighbors (or lower coordination number) than those in the core.

Independent evidence of the greater tendency to heterogeneity in the Au₂₅Pt₇₅ compared to that of Au₄₈Pt₅₂ can be obtained by measuring metal–metal distances by EXAFS. For both systems, we independently measured Pt–metal (Au, Pt) and Au–metal (Au, Pt) distances, defined as

$$R_{\text{Pt-M}} = x_{\text{Pt}}R_{\text{Pt-Pt}} + x_{\text{Au}}R_{\text{Pt-Au}} \quad (1)$$

$$R_{\text{Au-M}} = x_{\text{Au}}R_{\text{Au-Au}} + x_{\text{Pt}}R_{\text{Au-Pt}} \quad (2)$$

Even though the partial distances $R_{\text{Pt-Pt}}$, $R_{\text{Au-Au}}$, and $R_{\text{Pt-Au}} = R_{\text{Au-Pt}}$ cannot be obtained from the analysis for this system, they are expected to increase monotonically with Au composition, x_{Au} . Note that the x_{Au} here is not the same as the bulk concentration of Au (they are equal only if Au and Pt are homogeneously distributed in the sample). Furthermore, to a good approximation, the following relationship is expected to hold for Au/Pt alloys of all compositions, regardless of the heterogeneity and short-range order (due to the difference in lattice constant between Au and Pt)

$$R_{\text{Au-Au}} > R_{\text{Au-Pt}} > R_{\text{Pt-Pt}} \quad (3)$$

Therefore, as followed from eqs 2 and 3, the $R_{\text{Au-M}}$ should increase with x_{Au} . However, Table 1 demonstrates the opposite trend. In Au₂₅Pt₇₅, $R_{\text{Au-M}} = 2.84 \pm 0.01 \text{ \AA}$, while in Au₄₈Pt₅₂, $R_{\text{Au-M}} = 2.82 \pm 0.01 \text{ \AA}$. Thus, the contribution of Au–Au bonds in Au₂₅Pt₇₅ is weighted with the larger fraction than in the latter; that is only possible if that sample contains a large volume fraction of Au-rich regions (over which the Au–Au bonds contribute larger fraction to eq 2 compared to the bulk concentration of Au in the sample), and a small fraction of Au-deficient regions (which contribute little to eq 2 due to the small number of Au–Pt bonds). Such

segregation of Pt and Au inside the nanowires is consistent with the previous results obtained by the coordination number measurements that Au atoms prefer to cluster in the core region in the Au₂₅Pt₇₅ nanowires while in the Au₄₈Pt₅₂ samples they are more homogeneously distributed with Pt atoms.

By combining different characterization techniques such as TEM, EDS, UV–vis, and EXAFS, we have clearly shown that as-synthesized Au₂₅Pt₇₅ and Au₄₈Pt₅₂ nanowires are alloyed structures with the latter having homogeneous placement of Au and Pt atoms and the former a more highly ordered arrangement with a Pt-rich shell and an Au-rich core. It is interesting to consider how the heterogeneous Au₂₅Pt₇₅ alloy nanowires initially formed and how they subsequently evolved into homogeneous Au₄₈Pt₅₂. Here, we propose a growth mechanism that explains the formation of Au/Pt nanostructures with such a strong sensitivity to Au/Pt stoichiometry. In the synthesis of Au/Pt alloy nanomaterial, we believe that the standard reduction potential and surface free energy are the most important intrinsic parameters for determining the final heterogeneous nanostructures and lead to two competing mechanisms for the distribution of Au and Pt within the growing nanowire. On the one hand, the high values of standard reduction potential of Au and Pt in solution at room temperature ($E^{\Phi}(\text{Pt}^{2+}/\text{Pt}) = 1.20 \text{ V}$, $E^{\Phi}(\text{Au}^{3+}/\text{Au}) = 1.52 \text{ V}$) suggest that the Au³⁺ and Pt²⁺ ions are reduced quickly by the addition of excess amounts of NaBH₄ during the synthesis. However, since the reduction potential of Au is slightly higher than that of Pt, it is plausible that Au³⁺ would be reduced more easily during the nucleation and consequent growth stages and would consequently be found in the core, which forms first. On the other hand, surface free energy, defined by the change of the free enthalpy of the surface-creating process under an isothermal–isobaric condition, gives rise to an opposite trend for the Au/Pt atomic distribution compared to the reduction potential. The surface free energy of Au at room temperature (1.63 J/m²) is much lower than that of Pt (2.69 J/m²). This argument would then conclude that Au atoms would cluster near the surface of the product, while the Pt atoms are relegated to the sublayer or core region.⁵⁸

These competing growth mechanisms based on the standard reduction potential and surface free energy are further complicated by the interaction between metal surface and capping agent. It is well known that the capping agent (surfactant) is very important in the formation of nanomaterials during solution phase synthesis. For instance, alkaline carboxylic acids, alkylamines, alkylthiols, and alkylphosphines have all been used for the synthesis of transition metal/alloy and semiconductor nanomaterials with fine control over size, shape, and composition.^{3,6,7,41} The interaction between the surfactant and the metal surface is largely dependent on the electronegativity of the metal. Electronegativity describes the power of an atom to attract electrons to it. Fluorine (the most electronegative element) is assigned a value of 4.0, while cesium and francium, which are the least electronegative, have electronegativities of only 0.7. Since electronegativities of various atoms differ, that is, O > N >

S > Au > Pd > Pt, Pt atoms are then expected to show a relatively stronger interaction with octadecylamine ($C_{18}H_{36}NH_2$) than Au atoms, following from the increased probabilities of charge transfer from Pt and Au atoms to N atoms. As a consequence of preferential binding between octadecylamine and Pt metals surfaces, we suggest that the Pt atoms will be stabilized toward the surface and Au atoms will diffuse into core region, accounting for the formation of an Au_CPt_S (Au-core-rich and Pt-shell-rich) heterogeneous alloy. In fact, preferential binding between alkylamine or alkylthiol with Pd atoms have previously been reported to account for the formation of Au_CPd_S nonrandom alloy.^{59,60}

Supporting Information, Figure S5 shows that when the molar ratio of Au is low (e.g., $Au_{25}Pt_{75}$), the reduction rate of a relatively small portion of the Au^{3+} ions is even faster than that of most Pt^{2+} ions. Thus, it would lead to the preformation of Au-rich core, followed by sequential deposition of Pt to form Pt-rich shell. Furthermore, the preferential binding between octadecylamine and Pt atoms will further elevate the configuration of an Au-rich core and a Pt-rich shell, regardless of the low surface free energy of Au metal. When the molar ratio of Au is in the intermediate range (e.g., $Au_{48}Pt_{52}$), the reduction of Au^{3+} and Pt^{2+} occurs nearly spontaneously, resulting in the formation of AuPt nuclei with homogeneous Au and Pt distribution. Moreover, the tendency to form an Au-rich shell is promoted by the low surface free energy of Au, although it might be offset to some extent by the tendency to form a Pt-rich shell, promoted by the preferential binding between octadecylamine and Pt. We propose that this tension between two competing effects ultimately leads to the formation of a homogeneous Au/Pt alloy. Finally, when the molar ratio of Au is high (e.g., $Au_{75}Pt_{25}$), the equilibrium alloy phase diagram has evolved into to the biphase region, causing phase segregation between Au/Pt. Because of the low surface free energy, it is possible to nucleate particles of pure Au, further decreasing the concentration of Au in the solution. The equilibrium phase diagram then demands that the remaining Au atoms will form a homogeneous Au/Pt alloy.

The crystalline structure of $Au_{48}Pt_{52}$ and $Au_{25}Pt_{75}$ nanowires plays an important role in the electronic structure, evidenced by detailed analysis using X-ray absorption near-edge structure (XANES) spectroscopy. Upon the formation of alloyed nanostructure, electrons are transferred from the metal with the more occupied valence band to the metal with the less occupied band to stabilize the bimetallic bond. As an element-specific charge state probe, XANES is ideally suited to study the resulting electronic structure by comparing the changes in the intensity of the white lines (i.e., intense peaks at the L_3 absorption edges) from both the Pt and Au.⁵² Since Au metal has a filled d^{10} orbital, it usually does not exhibit an intense white line at L_3 edge thresholds, while Pt with its unfilled d^9 orbital normally would. The orbital s-p-d hybridization of Au metal results in a $5d^{10-x}6(sp)^{1+x}$ electron configuration, leading to a noticeable change of white line intensity. Figure 3 shows normalized Pt L_3 and Au L_3 edge XANES spectra of Au/Pt nanowires and those of Au and Pt foils as references. For $Au_{48}Pt_{52}$ nanowires, the strength of

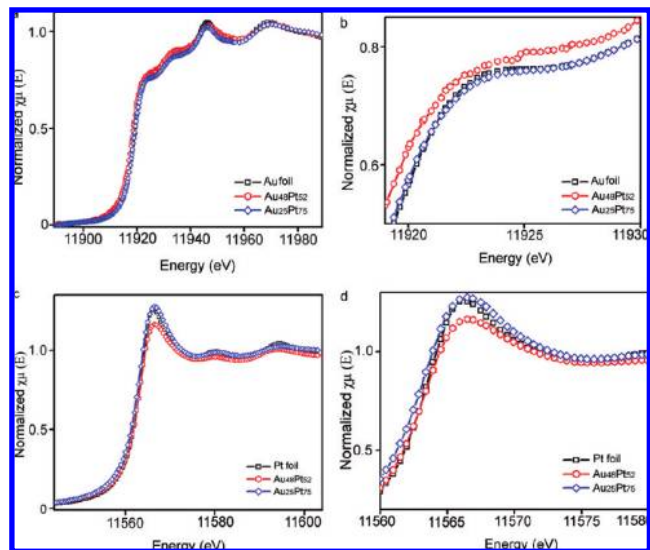


Figure 3. XANES spectrum of as-made $Au_{48}Pt_{52}$ (nanowires), $Au_{25}Pt_{75}$ (nanowires), Pt (foil reference), and Au (foil reference).

the Au white line feature is noticeably higher than that of pure Au foil. Since features in the white line at the Au L_3 edge arise from $2p_{3/2}$ to $5d_{5/2}$ dipole transitions, our observations indicate a decrease in the number of unoccupied states of d character at the Au site upon the $Au_{48}Pt_{52}$ alloy formation. An opposite trend is seen at the Pt L_3 edge, where the white line feature is lower than that of the pure Pt foil. The Pt and Au L_3 edges shifted in opposite directions are the consequence of Au/Pt alloy formation. The data can be further interpreted in terms of the hole population above the Fermi level, in which sense the d-charge depletion at the Au site is accompanied by the d-charge gain at the Pt site. Electronic charge neutrality requires that the d-charge gain at the Pt site should be comparable to the charge loss at the Au sites. In contrast, the Au and Pt white line features found in $Au_{25}Pt_{75}$ nanowires are very close to those found in Au and Pt foil. The bulklike XANES curves around the absorption edge indicate no apparent charge transfer between Au and Pt atoms, as well as between Au/Pt and octadecylamine in $Au_{25}Pt_{75}$ nanowires. The electronic structure of AuPt alloy nanoparticles supported on the metal oxides has been studied by Van Bokhoven and co-workers,⁶¹ finding a charge transfer between Au and Pt similar to our results on Au/Pt free-standing nanowires. However, the charge transfer of Au/Pt phase-segregated nanostructures is totally different from that of an alloyed structure. Very recently, we have reported the charge transfer of a Au/Pt hybrid with complete Au and Pt phase-segregation,³⁵ finding d-charge depletion at the Pt site and d-charge gain at the Au site. We believe that the distinct electronic structures found in the two materials can be attributed to their different crystalline structures. Since Au has a higher electronegativity than Pt, in Au/Pt hybrid phase-segregated nanowires Pt loses electrons to Au. In Au/Pt alloyed nanowires, alloying between Au and Pt drives the system toward the “covalent limit”, where the d bandwidth is much larger than the energy separation of the d bands, forcing Pt and Au toward equal electron counts in the alloy.⁶¹ These findings dramatically highlight the intriguing

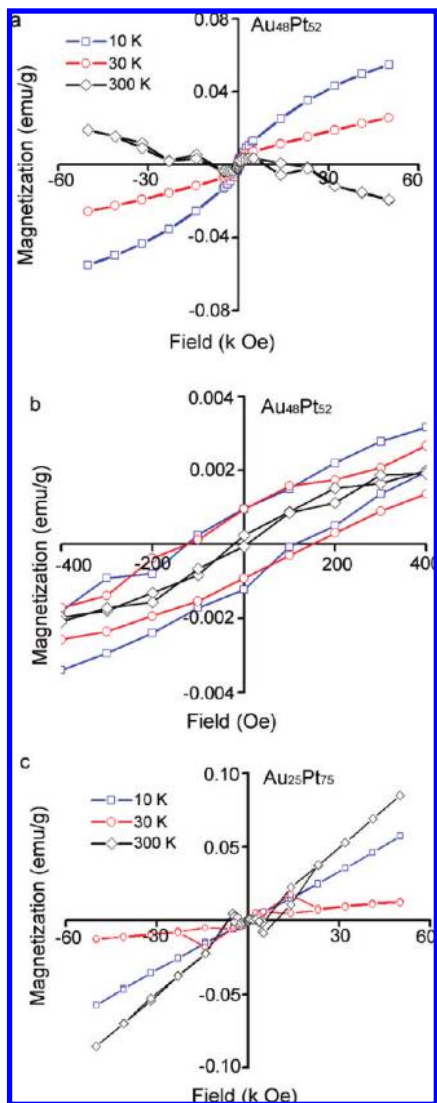


Figure 4. Field-dependent magnetization of $\text{Au}_{48}\text{Pt}_{52}$ and $\text{Au}_{25}\text{Pt}_{75}$ nanowires measured at 10, 30, and 300 K.

ing structure–property relationship of nanoscaled electronic materials.

In order to determine if the charge transfer can induce ferromagnetism in Au/Pt nanowires, we carried out magnetization measurements for our two samples with a quantum design magnetic property measurement system (MPMS). The dried powders of samples were contained in gelatin capsules fastened in plastic straws for immersion into the magnetometer. No subtraction of the diamagnetic signal from the sample container was made for the magnetization data. Figure 4a shows the magnetization as a function of applied magnetic field at 10, 30, and 300 K for the $\text{Au}_{48}\text{Pt}_{52}$ nanowires. At 10 and 30 K, the magnetization at high positive fields is positive and is not saturated even in 55 kOe. At 300 K the magnetization changes its field dependence and becomes negative in high positive fields. However, at lower fields the magnetization shows pronounced nonlinearities and a non-zero coercive field at all temperatures measured (see Figure 4b). Thus, we conclude that the magnetization of $\text{Au}_{48}\text{Pt}_{52}$ nanowires consists of both ferromagnetic and paramagnetic components. The ferromagnetic component gradually de-

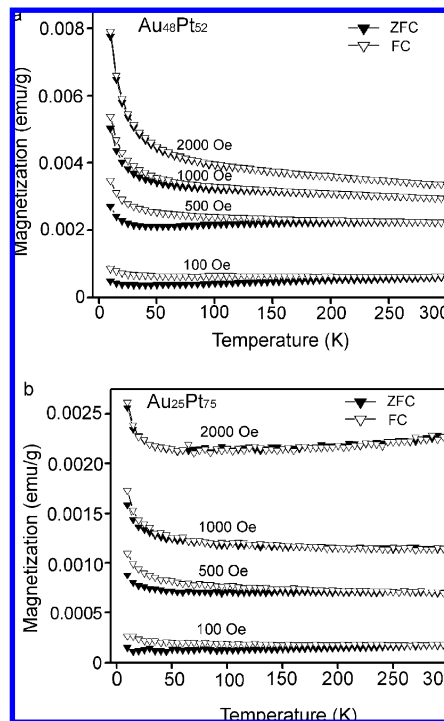


Figure 5. Temperature-dependent magnetizations (ZFC and FC) of $\text{Au}_{48}\text{Pt}_{52}$ and $\text{Au}_{25}\text{Pt}_{75}$ nanowires measured under applied fields of 100, 500, 1000, and 2000 Oe, respectively.

creases as the temperature increases, and eventually is overwhelmed at 300 K by the diamagnetic contribution from the sample container. The results of similar magnetization measurements on the $\text{Au}_{25}\text{Pt}_{75}$ nanowires are different. Figure 4c shows that the magnetization is linear as a function of the field with a positive slope at all temperatures and it shows no coercivity at low fields at all temperatures. Thus, the magnetization of $\text{Au}_{25}\text{Pt}_{75}$ nanowires consists of the paramagnetic component only. Remarkable the magnitudes of the magnetization in both samples are very similar at all fields and temperatures, despite very different compositions.

In order to further investigate the magnetic properties of Au/Pt nanowires, we performed measurements of the temperature-dependent magnetization from 10 to 300 K. We used the standard zero-field cooled (ZFC) and field-cooled (FC) protocols at different applied fields ranging from 100 to 2000 Oe as shown in Figure 5. The temperature-dependent magnetizations show similar trends in both samples. The magnetizations in the higher fields are approximately temperature-independent at high temperatures, but increase rapidly with decreasing temperature. The ZFC and FC values for the temperature-dependent magnetization have interesting field-dependencies. In fields larger than ~ 1000 Oe, no hysteresis is observed at any temperature for the ZFC and FC curves of either composition of Au/Pt nanowire. At lower fields, there is an increasing departure of the FC and ZFC curves. These data also imply that the magnetization contains two components. The first one is temperature-dependent with Curie-like behavior at low temperatures, while the second one is temperature-independent and dominates at higher temperature.

The magnetic properties of Au/Pt nanowires are driven not only by their Au/Pt composition, but also by finite size effects. The most prominent finite size effect is the presence of the canted spins on the surface of nanowires, which in some cases might account for the nonsaturation of the magnetization at high magnetic fields.^{62,63} We will show that this is also the case for our samples.

Unlike the case of the bulk paramagnet where the magnetization is identical and fully reversible for field-cooled and zero-field cooled measurements, the clear signs of irreversibility demonstrated in Figure 5 show that these canted spins have a complex and metastable configuration that depends on the prior field and temperature history. Such behavior is not unusual in magnetic nanoparticle systems.⁸ The suppression of this metastability in large fields signals that here the moments have been forced into a reversible and overall aligned configuration. The fact that this critical field is the same for both samples suggests that the number of canted spins is similar for both nanowires, which is reasonable considering their similar size.

Our most striking result is the observation of ferromagnetism in the Au₄₈Pt₅₂ nanowires. Several factors have been proposed to explain the onset of ferromagnetism in late 4d and 5d transition metals and in Pd, Pt, and Au in particular.^{21,23,28,30,64,65} For example, the density of states at the Fermi level may be enhanced in some materials by decreasing particle size, enabling a fulfillment of the Stoner criterion for ferromagnetism in a way which is impossible for the bulk material. Alternatively, it is possible that the low ferromagnetic moments observed in those 4d and 5d metals arises from a very small fraction of the total number of atoms, probably located at the surface of a nanoparticle, where the electronic structure is sufficiently different from that of the bulk to enable moment stabilization and even ferromagnetism of these surface spins. We note that the reduced coordination number of surface atoms, especially at defect sites, may also induce large spin-orbit coupling, known to stabilize ferromagnetic behavior on the nanoscale. Finally, the covalent interaction between metal nanoparticles and capping agents (surfactants) may also result in localized electronic charge at the nanoparticle surface, as found in several studies of Pd, Au, and ZnO nanoparticles, where the capping agent (thiol group) strongly attracted electrons from the metal surface,^{23,25,29} resulting in an increase in the density of holes at the metal surface. While the exact mechanism remains obscure, it is an appealing hypothesis that these charged surface states are somehow crucial for moment formation, fueling the ferromagnetic instabilities that are found in nanoscaled metals. However, our XANES work shows that there is apparently little charge transfer between Au/Pt and octadecylamine, as evidenced by the bulklike white line intensity observed in Au₂₅Pt₇₅, and the relatively strong charge transfer from Au to Pt was observed in Au₄₈Pt₅₂ nanowires. Our magnetization measurements show the Curie-like behavior of the canted surface spins in both samples, thus it is unlikely that the canted spins would explain a nonzero coercivity of Au₄₈Pt₅₂ nanowires.

The hysteresis-like behavior of the magnetization of Au₄₈Pt₅₂ nanowires at all temperatures signals a close proximity to ferromagnetism in Au₄₈Pt₅₂ ultrathin nanowires, where the homogeneous Au and Pt distribution places a greater number of Au and Pt atoms close to each other. This improves the net charge transfer from Au to Pt, which in this picture stabilizes moment-bearing holes on the Au atoms. In contrast, the relative segregation effected by the Au-core-rich and Pt-shell-rich configuration found in the Au₂₅Pt₇₅ heterogeneous nanowires does not permit the same degree of average charge transfer, and the Au atoms remain nonmagnetic with the simple Pauli paramagnetism found in nanosized Au. Note that the observed ferromagnetism in Au₄₈Pt₅₂ homogeneous alloy is unique for the ultrathin nanowires with an average width of 2.6 ± 0.4 nm, showing strong size and stoichiometry dependencies. Larger Au/Pt and Au₂₅Pt₇₅ nanowires appear to have heterogeneous crystalline configurations, suggesting that here there will not be the same degree of charge transfer between Au and Pt atoms as is found in homogeneous Au₄₈Pt₅₂ nanowires. Thus, paramagnetism (from Pt) and diamagnetism (from Au) will be exhibited instead of ferromagnetism.

In summary, we have synthesized and characterized Au/Pt alloyed nanowires with heterogeneous structures that depend strongly on the Au/Pt stoichiometry. Ferromagnetic moments are stabilized in Au₄₈Pt₅₂ nanowires, driven by enhanced Au-Pt charge transfer. We have presented here a comprehensive study of the relationships among heterogeneous crystalline structure, electronic structure, and magnetic behavior, and our results address the most fundamental issues regarding the electronic instabilities of a 1D nanomaterial. Our studies are highly encouraging that new families of bimetallic nanosystems may be developed to sustain the needs of emerging technologies such as spintronics and data storage, where there is a continuous drive to find nanomaterials with ever more exotic electronic and magnetic properties, and where the assembly of these fundamental building blocks can lead to new types of functionality. The extent to which ferromagnetism driven by enhanced charge transfer between Au and Pt atoms can be observed in forms of Au/Pt nanomaterials other than nanowires is not entirely clear at this moment. It will deserve further investigations in the near future.

Acknowledgment. This work is supported by the University of New Hampshire. A.I.F. and Q.W. acknowledge support by the U.S. Department of Energy Grant DE-FG02-03ER15476. Use of the National Synchrotron Light Source, Brookhaven National Laboratory, was supported by the U.S. Department of Energy, Office of Science, Office of Basic Energy Sciences, under Contract DE-AC02-98CH10886 and beamlines X19A/X18B are partly supported by Synchrotron Catalysis Consortium under contract DE-FG02-05ER15688. Part TEM work was performed in the EPIC facility of the NUANCE center at Northwestern University.

Supporting Information Available: Descriptions of materials synthesis and characterizations and EDS analysis of large area of Au/Pt nanowires assemblies (Figure S1),

the UV–vis absorption spectrum of as-made nanowires and mixture of nanowires and Au nanoparticles (Figure S2), TEM images of Au₂₅Pt₇₅ Au₄₈Pt₅₂ nanowires and mixture of nanowires and nanoparticles (Figure S3), the Fourier transform magnitudes of k₂ weighted EXAFS data and theoretical fits for Pt and Au L₃ edges of Au₂₅Pt₇₅ and Au₄₈Pt₅₂ (Figure S4), schematic drawing of the growth mechanism of Au/Pt heterogeneous nanostructures (Figure S5), and enlarged images of ZFC/FC curves measured at 100 and 2000 Oe for both nanowires (Figure S6). This material is available free of charge via the Internet at <http://pubs.acs.org>.

References

- O’Handley, R. C. *Modern Magnetic Materials: Principles and Applications*; John Wiley & Sons, Inc.: New York, 2000.
- Thompson, D. A.; Best, J. S. *IBM J. Res. Dev.* **2000**, *44*, 311–322.
- Hyeon, T. *Chem. Commun.* **2003**, xxx927–934.
- Bader, S. D. *Rev. Mod. Phys.* **2006**, *78*, 1–15.
- Sun, S. H. *Adv. Mater.* **2006**, *18*, 393–403.
- Jeong, U.; Teng, X. W.; Wang, Y.; Yang, H.; Xia, Y. N. *Adv. Mater.* **2007**, *19*, 33–60.
- Lu, A. H.; Salabas, E. L.; Schuth, F. *Angew. Chem., Int. Ed.* **2007**, *46*, 1222–1244.
- Kodama, R. H. *J. Magn. Magn. Mater.* **1999**, *200*, 359–372.
- Neel, L. J. *Phys. Radium* **1954**, *15*, 376–378.
- Skomski, R. J. *Phys.: Condens. Matter* **2003**, *15*, R841–R896.
- Mermin, N. D.; Wagner, H. *Phys. Rev. Lett.* **1966**, *17*, 1133.
- Bander, M.; Mills, D. L. *Phys. Rev. B* **1988**, *38*, 12015–12018.
- Zhu, M. J.; Bylander, D. M.; Kleinman, L. *Phys. Rev. B* **1990**, *42*, 2874–2877.
- Blugel, S. *Phys. Rev. Lett.* **1992**, *68*, 851–854.
- Blugel, S. *Phys. Rev. B* **1995**, *51*, 2025–2028.
- Taniyama, T.; Ohta, E.; Sato, T. *Europhys. Lett.* **1997**, *38*, 195–200.
- Delin, A.; Tosatti, E. *Phys. Rev. B* **2003**, *68*, 144434.
- Sampedro, B.; Crespo, P.; Hernandez, A.; Litran, R.; Lopez, J. C. S.; Cartes, C. L.; Fernandez, A.; Ramirez, J.; Calbet, J. G.; Vallet, M. *Phys. Rev. Lett.* **2003**, *91*, 237203.
- Shinohara, T.; Sato, T.; Taniyama, T. *Phys. Rev. Lett.* **2003**, *91*, 197201.
- Delin, A.; Tosatti, E.; Weht, R. *Phys. Rev. Lett.* **2004**, *92*, 057201.
- Hori, H.; Yamamoto, Y.; Iwamoto, T.; Miura, T.; Teranishi, T.; Miyake, M. *Phys. Rev. B* **2004**, *69*, 174411.
- Alexandre, S. S.; Anglada, E.; Soler, J. M.; Yndurain, F. *Phys. Rev. B* **2006**, *74*, 054405.
- Litran, R.; Sampedro, B.; Rojas, T. C.; Multigner, M.; Sanchez-Lopez, J. C.; Crespo, P.; Lopez-Cartes, C.; Garcia, M. A.; Hernandez, A.; Fernandez, A. *Phys. Rev. B* **2006**, *73*, 054404.
- Garcia, M. A.; Ruiz-Gonzalez, M. L.; de la Fuente, G. F.; Crespo, P.; Gonzalez, J. M.; Llopis, J.; Gonzalez-Calbet, J. M.; Vallet-Regi, M.; Hernandez, A. *Chem. Mater.* **2007**, *19*, 889–893.
- Coey, J. M. D.; Wongsaprom, K.; Alaria, J.; Venkatesan, M. *J. Phys. D: Appl. Phys.* **2008**, *41*, 134012.
- Stoner, E. C. *Philos. Mag.* **1924**, *48*, 719–736.
- Liu, X.; Bauer, M.; Bertagnolli, H.; Roduner, E.; van Slageren, J.; Philipp, F. *Phys. Rev. Lett.* **2006**, *97*, 049902.
- De La Venta, J.; Pinel, E. F.; Garcia, M. A.; Crespo, P.; Hernandez, A. *Mod. Phys. Lett. B* **2007**, *21*, 303–319.
- Garcia, M. A.; Merino, J. M.; Pinel, E. F.; Quesada, A.; de la Venta, J.; Gonzalez, M. L. R.; Castro, G. R.; Crespo, P.; Llopis, J.; Gonzalez-Calbet, J. M.; Hernandez, A. *Nano Lett.* **2007**, *7*, 1489–1494.
- Angappane, S.; Park, J.; Jang, Y. J.; Hyeon, T.; Park, J. G. *J. Phys.: Condens. Matter* **2008**, *20*, 295209.
- Smogunov, A.; Dal Corso, A.; Delin, A.; Weht, R.; Tosatti, E. *Nat. Nanotechnol.* **2008**, *3*, 22–25.
- Teng, X. W.; Han, W. Q.; Ku, W.; Hucker, M. *Angew. Chem., Int. Ed.* **2008**, *47*, 2055–2058.
- Brinkman, A.; Huijben, M.; Van Zalk, M.; Huijben, J.; Zeitler, U.; Maan, J. C.; Van der Wiel, W. G.; Rijnders, G.; Blank, D. H. A.; Hilgenkamp, H. *Nat. Mater.* **2007**, *6*, 493–496.
- Suber, L.; Fiorani, D.; Scavia, G.; Imperatori, P.; Plunkett, W. R. *Chem. Mater.* **2007**, *19*, 1509–1517.
- Teng, X. W.; Han, W. Q.; Wang, Q.; Li, L.; Frenkel, A. I.; Yang, J. C. *J. Phys. Chem. C* **2008**, *112*, 14696–14701.
- Liang, H. P.; Guo, Y. G.; Zhang, H. M.; Hu, J. S.; Wan, L. J.; Bai, C. L. *Chem. Commun.* **2004**, xxx1496–1497.
- Luo, J.; Njoki, P. N.; Lin, Y.; Wang, L. Y.; Zhong, C. J. *Electrochem. Commun.* **2006**, *8*, 581–587.
- Zhou, S. H.; Jackson, G. S.; Eichhorn, B. *Adv. Funct. Mater.* **2007**, *17*, 3099–3104.
- Chen, J. Y.; Herricks, T.; Geissler, M.; Xia, Y. N. *J. Am. Chem. Soc.* **2004**, *126*, 10854–10855.
- Chen, J. Y.; Herricks, T.; Xia, Y. N. *Angew. Chem., Int. Ed.* **2005**, *44*, 2589–2592.
- Xia, Y.; Xiong, Y. J.; Lim, B.; Skrabalak, S. E. *Angew. Chem., Int. Ed.* **2009**, *48*, 60–103.
- Xia, Y. N.; Halas, N. J. *MRS Bull.* **2005**, *30*, 338–344.
- Xia, Y. N.; Yang, P. D.; Sun, Y. G.; Wu, Y. Y.; Mayers, B.; Gates, B.; Yin, Y. D.; Kim, F.; Yan, Y. Q. *Adv. Mater.* **2003**, *15*, 353–389.
- Rao, C. N. R.; Deepak, F. L.; Gundiah, G.; Govindaraj, A. *Prog. Solid State Chem.* **2003**, *31*, 5–147.
- Burda, C.; Chen, X. B.; Narayanan, R.; El-Sayed, M. A. *Chem. Rev.* **2005**, *105*, 1025–1102.
- Cozzoli, P. D.; Manna, L. *Nat. Mater.* **2005**, *4*, 801–802.
- Jana, N. R.; Gearheart, L.; Murphy, C. J. *Chem. Commun.* **2001**, xxx617–618.
- Murphy, C. J.; Jana, N. R. *Adv. Mater.* **2002**, *14*, 80–82.
- Sun, Y. G.; Xia, Y. N. *Adv. Mater.* **2002**, *14*, 833–837.
- Maksimuk, S.; Teng, X. W.; Yang, H. *Phys. Chem. Chem. Phys.* **2006**, *8*, 4660–4663.
- Gou, L. F.; Murphy, C. J. *Chem. Mater.* **2005**, *17*, 3668–3672.
- Durham, P. J.; Pendry, J. B.; Hodges, C. H. *Comput. Phys. Commun.* **1982**, *25*, 193–205.
- Frenkel, A. I.; Hills, C. W.; Nuzzo, R. G. *J. Phys. Chem. B* **2001**, *105*, 12689–12703.
- Newville, M. J. *Synchrotron Radiat.* **2001**, *8*, 322–324.
- Zabinsky, S. I.; Rehr, J. J.; Ankudinov, A.; Albers, R. C.; Eller, M. J. *Phys. Rev. B* **1995**, *52*, 2995–3009.
- Frenkel, A. Z. *Kristallogr.* **2007**, *222*, 605–611.
- Menard, L. D.; Wang, Q.; Kang, J. H.; Sealey, A.; Girolami, G. S.; Teng, X. W.; Frenkel, A. I.; Nuzzo, R. G., to be submitted.
- Mezey, L. Z.; Giber, J. *Jpn. J. Appl. Phys.* **1982**, *21*, 1569–1571.
- Knecht, M. R.; Weir, M. G.; Frenkel, A. I.; Crooks, R. M. *Chem. Mater.* **2008**, *20*, 1019–1028.
- Teng, X. W.; Wang, Q.; Liu, P.; Han, W.; Frenkel, A.; Wen, W.; Marinkovic, N.; Hanson, J. C.; Rodriguez, J. A. *J. Am. Chem. Soc.* **2008**, *130*, 1093–1101.
- Bus, E.; van Bokhoven, J. A. *J. Phys. Chem. C* **2007**, *111*, 9761–9768.
- Coey, J. M. D. *Phys. Rev. Lett.* **1971**, *27*, 1140.
- Morales, M. P.; Serna, C. J.; Bodker, F.; Morup, S. J. *Phys.: Condens. Matter* **1997**, *9*, 5461–5467.
- Yamamoto, Y.; Miura, T.; Suzuki, M.; Kawamura, N.; Miyagawa, H.; Nakamura, T.; Kobayashi, K.; Teranishi, T.; Hori, H. *Phys. Rev. Lett.* **2004**, *93*, 116801.
- Hernando, A.; Crespo, P.; Garcia, M. A.; Pinel, E. F.; de la Venta, J.; Fernandez, A.; Penades, S. *Phys. Rev. B* **2006**, *74*, 052403.

NL9013716